Ann. Rev. Phys. Chem. 1983. 34 : 389–417

MAGNETIC FIELD EFFECTS ON REACTION YIELDS IN THE SOLID STATE: An Example from Photosynthetic Reaction Centers

Steven G. Boxer, Christopher E. D. Chidsey, and Mark G. Roelofs

Department of Chemistry, Stanford University, Stanford, California 94305

INTRODUCTION

Magnetic Field Effects

Prior to 1970 there were several reports of the effects of magnetic fields on chemical reactions, though there was much rebuttal and retraction in this early literature (1–3). Since 1970, the number of reproducible examples has grown rapidly. Most contemporary theories explaining these effects stem from the development of the radical pair theory of Chemically Induced Dynamic Nuclear Polarization, CIDNP (4, 5). These are based on the interconversion of spin multiplets through the action of inhomogeneous magnetic fields, hyperfine interactions, or differences in the g factors of the chemical species involved. Most systems that exhibit magnetic field effects involve reactions of radical pairs, though other examples, such as the interconversion of ortho and para hydrogen (3), luminescence arising from triplet-triplet annihilation (6), and quenching of triplet states by radicals (7), are well documented.

A good example of the effect of a magnetic field on a reaction involving radical pairs in solution is the pioneering work by Schulten & Weller and Michel-Beyerle & Haberkorn on triplets formed by the recombination reaction between pyrene anions ($^2Py^-$) and dimethylanaline cations ($^2Dma^+$) (8–13) shown in Figure 1. Applied magnetic fields decrease the

0066–426X/83/1101–0389$02.00

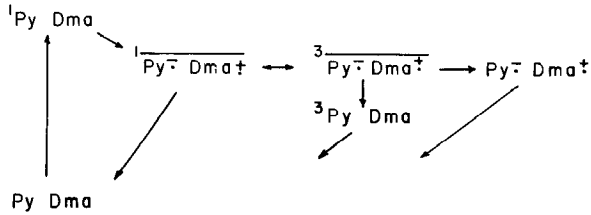

Figure 1 Reaction scheme for the quenching of pyrene (Py) singlet excited states by dimethylanaline (Dma). Py triplets are formed exclusively by annihilation of ion pairs when the concentration of Dma is large enough to quench all singlet excited pyrenes.

yield of triplet states, ^{3}Py. The effect of the magnetic field is saturated by 250 G and corresponds to a 14% decrease in the intensity of delayed fluorescence (due to triplet-triplet annihilation) over that at zero magnetic field. A parameter characterizing the field dependence is $B_{1/2}$, defined as the field that gives one half of the maximum decrease in intensity of delayed fluorescence. $B_{1/2}$ is 55 G for this system. $B_{1/2}$ values are widely used to characterize magnetic field effects; however, the reader is cautioned that the full shape of the field dependence of the yield contains considerably more information, as is seen below.

A theory similar to that used in CIDNP was developed to explain the effect of the magnetic field (8–13). The explanation in qualitative terms is as follows: The initial state of the radical pair is a singlet, but only triplet radical pairs can give rise to the molecular triplet state ^{3}Py. The energies of the four electron spin states of a weakly coupled radical pair as a function of applied magnetic field strength are shown in Figure 2. If the exchange interaction and electron-dipole electron-dipole coupling between the radicals are weak, then all three triplet levels and the singlet level are effectively degenerate at zero field. Transitions between singlet and all three triplet states of the radical pair can be induced by magnetic hyperfine

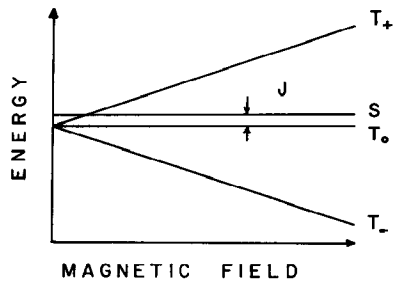

Figure 2 Energy levels for a radical pair as a function of applied magnetic field strength in the absence of electron-dipole electron-dipole interactions, but with a small isotropic exchange interaction, J, leading to a small singlet-triplet splitting.

interactions. At higher magnetic fields only the S and T_0 levels are energetically close to each other, and the energy difference between S and T_+ or between S and T_- prevents mixing of these states. This results in a decrease in the quantum yield of molecular triplets in a magnetic field compared to the yield at zero magnetic field.

Quantitative proof that the hyperfine mechanism was responsible for singlet-triplet mixing in the radical pair came from the agreement between experimental and theoretically prediced $B_{1/2}$ values (55 G experimental, 59 G predicted) (11). Furthermore, $B_{1/2}$ was much smaller for the *perdeuterated* molecules (27 G, experimental, 21 G predicted) (11). In fluid solution the exchange and dipolar interactions between the radicals are negligible due to diffusion, and $B_{1/2}$ is determined primarily by the strength of the hyperfine interactions. Deuteration reduces the strength of the hyperfine interactions and thus the strength of the applied magnetic field necessary to prevent the singlet radical pair state S from mixing with T_+ or T_-.

There are several other related kinds of magnetic effects. The decay kinetics of radical pairs can depend on field strength if singlet and triplet radical pairs decay at different rates. Nuclear spin polarization (CIDNP) is obtained because certain nuclear states cause more efficient S-T mixing (4, 5). Electron spin polarization (CIDEP) can be generated, and this effect has been seen in photosynthetic systems for both triplet products (13a) and chemically inert, nearby radicals that communicate via spin exchange with radical pairs (13b). Resonant radio frequency magnetic fields can cause changes in the reaction yield (reaction yield detected magnetic resonance, RYDMR), as has been observed in a variety of systems (13c,d), including photosynthetic systems (13e,f). Finally, isotope fractionation between triplet and singlet products can result from differing nuclear magnetic moments (14–16).

Diffusion can play a crucial role in radical pair reactions. Relative translational diffusion is important because it modulates radical pair creation and decay reactions and spin-spin interactions. Rotational diffusion causes averaging of anisotropic interactions and populations. It is the absence of these diffusive effects on some relevant time scale which is our operational definition of a "solid state" reaction in this review.

Primary Photochemistry of Photosynthesis

The only well-developed example of a radical pair reaction in the solid state whose outcome can be influenced by magnetic fields comes from photosynthetic systems. There are a number of interesting parallels with amorphous Si; however, because electron-hole pairs migrate in this material, it is phenomenologically more similar to solution (17–20).

Another example is electron injection from adsorbed dye molecules (e.g. rhodamine B) into anthracene crystals (21). Although the analysis of photosynthesis is not the primary purpose of this review, this system is interesting and serves as our example of the kinds of structural and mechanistic insight that can be gained by studying magnetic field effects in solids.

Photosynthesis is a complex series of chemical transformations initiated by photoinduced electron transfer forming a cation-anion radical pair. We are only concerned with this most primary step here, which appears to be general for photosystems I and II of green plants and algae and bacterial photosynthesis. The site of this primary photochemistry is called a reaction center (RC), which consists of several chlorophyll-type chromophores, quinones and other electron carriers, intimately associated with an integral membrane protein. The best characterized and simplest RC is obtained from the purple bacterium *Rhodopseudomonas spheroides*, R-26 mutant, and all further discussion of RCs relates to this system (22–24). The precise nature and spatial arrangement of the chlorophyll-type chromophores that serve as both electron donors and acceptors are very active areas of study. The details need not concern us, except to note that the initially formed cation-radical (denoted $P^{\ddagger}$) and anion-radical (denoted $I^{\ddagger}$) are aromatic radical ions (chlorophyll π-radicals) (25) and that they are immobilized in the RC complex.

As the RC is excised from the functional organism, its chemistry is limited to the first few steps of photosynthesis. The kinetics of these steps are shown schematically in Figure 3A. The absorption of light by P at about 870 nm leads to the rapid formation of $P^{\ddagger}I^{\ddagger}$ (26–31); the quantum yield of this reaction is nearly unity (32). The secondary reductions of the quinones are slower, producing increasingly stable ion-pairs (26, 27, 32–36). The secondary reaction: $P^{\ddagger}I^{\ddagger}Q_AQ_B \rightarrow P^{\ddagger}IQ_A^{\ddagger}Q_B$ can be blocked by removing Q altogether or prior chemical reduction to $Q_A^{\ddagger}$ or Q_A^{2-}. These three methods of blocking the chemistry are distinctly different as $Q_A^{\ddagger}$ is charged and paramagnetic, whereas Q_A^{2-} is doubly charged and diamagnetic; we will consider principally the simplest case in which Q_A is removed. The fate of the initial radical pair, $P^{\ddagger}I^{\ddagger}$, is now more complex, as shown in Figure 3B. In addition to recombination to the singlet ground state, reaction to the molecular triplet, ^3P, is possible (the triplet yield, Φ_T, is about 0.2 at room temperature and nearly 1 below 100 K) (13a, 37–39). An *S-T* mixing mechanism in the radical ion pair is necessary in order to produce ^3P. It is evident that the schemes in photosynthesis shown in Figure 3B and that for Py/Dma in Figure 1 are nearly identical. The fundamental difference is that the radicals are not free to diffuse in the RC; thus the electron-electron exchange interaction does not vanish and all anisotropic magnetic

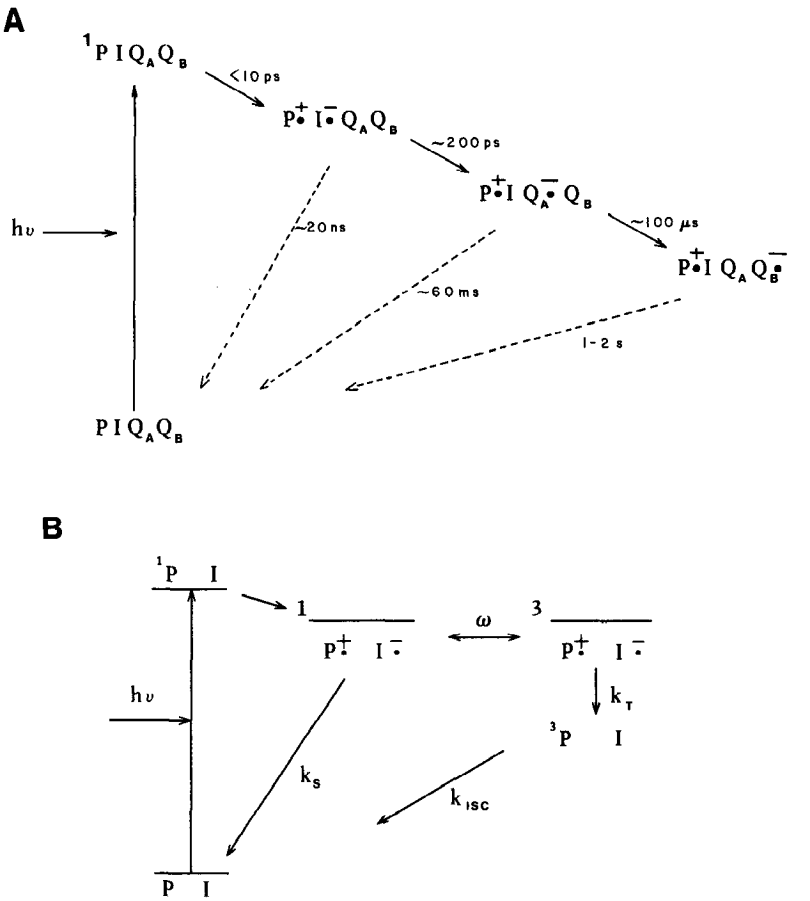

Figure 3 Kinetic scheme for the primary intermediates in bacterial photosynthesis. (A) Kinetics in functional reaction centers; (B) kinetics in blocked reaction centers. *Horizontal bars* are used to denote spin-correlated radical pairs.

characteristics of P^+I^- must be considered. These produce novel magnetic field effects, which are the main thrust of this review.

Magnetic Field Effects in Photosynthetic Reaction Centers

In 1977 Parson & Hoff and their co-workers observed that the quantum yield of ^3P in blocked RCs was *decreased* by the application of a magnetic field (40, 41). The decrease was monotonic with increasing field and the effect saturated (no further decrease with increasing field) by 2 kG, where

the quantum yield was 60% of that in the absence of a field. The theory described above for radical recombination in solution was adapted to the RC problem by Schulten and Haberkorn and their co-workers (42, 43), with the additional assertion that the exchange interaction between $P^{+\cdot}$ and $I^{-\cdot}$ would be finite and constant in time, as the reactants are not free to diffuse. The observed magnetic field effect then led to the important conclusion that the exchange interaction between $P^{+\cdot}$ and $I^{-\cdot}$ was small (less than 100 G, 10^{-6} eV). A review of this important work has been presented by Hoff (43a). It was also reported that the triplet yield in deuterated $Q_A^{-\cdot}$-containing RCs is identical to that in protonated RCs (39, 44), a perplexing result in light of the results in solution discussed above.

More information can be obtained from the effect of high ($H > 1$ kG) magnetic fields, where the difference in the g-factors of $P^{+\cdot}$ and $I^{-\cdot}$ (Δg) leads to an *increased* rate of singlet to triplet conversion in the radical pair state and an increased triplet yield (45, 46). The "Δg-effect" can be qualitatively visualized by reference to the classical spin precession vector model shown in Figure 4. S and T_0 differ in this picture only in the relative phase of the two spins. The effective magnetic field at each electron determines its precession frequency and thus the evolution in time of the spin correlation: from S to T_0 and back. For fields of a few thousand Gauss, the magnitude of the difference in precession frequency (ω) for a typical set of nuclear states is determined predominantly by hyperfine interactions. However, if Δg is not zero, its contribution to ω at very large magnetic fields increases and can become dominant.

The effect of increasing ω on the triplet quantum yield can be seen by reference to the kinetic scheme for triplet formation in Figure 3B. The radical pair is formed initially in a singlet state. Singlet recombination with rate constant k_S competes with singlet-triplet conversion at frequency ω. An increase in ω should increase the yield of triplet radical pairs, if ω does not exceed k_T, and thus of molecular triplets, ^3P. At sufficiently large magnetic

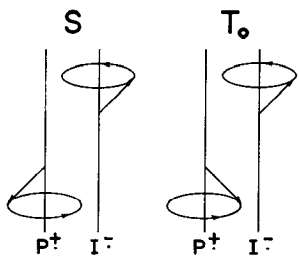

Figure 4 Vector model for precession of spins in a radical pair at high magnetic field strength. The spin on $I^{-\cdot}$ may be precessing either slower or faster than that on $P^{+\cdot}$. The $S \rightarrow T_0$ conversion requires no spin flips, but only a change in the relative phase of the two electrons.

fields, ω will exceed both k_S and k_T, and the two radical pair states are described as an equilibrium system drained by two decay reactions. In this limit the yield is expected to become independent of magnetic field and is given by $k_T/(k_S+k_T)$. The reader is cautioned that the "infinite field limit" is often mentioned in the literature on magnetic field effects for fields at which the low field effect saturates, carelessly neglecting the Δg-effects (43a). Even though the effect is very well known from the CIDNP literature, Δg effects have been much less widely studied for solution phase reactions. As is seen below, an important advantage of using the Δg-effect is that an analytical theory can be developed with few approximations, in contrast to the situation at low field for which calculations become especially difficult when anisotropic interactions must be considered (47).

The solid state nature of the RC leads to the notion that the yield of triplets might also depend upon the orientation of RCs in a magnetic field (48, 49); we have called this the *quantum yield anisotropy*. In the high-field limit (electron Zeeman interaction much greater than the spin-spin interactions, $H > 1000$ G) the radical-pair energy-level diagram reduces to a simple two-level system, S and T_0. The energy difference between these two states is due to the isotropic exchange and the orientation-dependent electron-dipole electron-dipole interactions. Because S-T_0 mixing is impeded by an energy difference between the two states, RCs with different orientations in a magnetic field should have different triplet quantum yields. In addition, the nuclear hyperfine interactions and the g-factor difference which drive S-T_0 mixing are likely to be anisotropic. Because the contribution of the g-factor difference to the rate of S-T_0 mixing increases with increasing field, whereas that due to hyperfine interactions and the inhibition due to the S-T_0 energy difference are constant with field strength, the anisotropy of Φ_T may change dramatically with field. This anisotropy is expected to decrease to zero at extremely large fields, as Φ_T is no longer limited by the S-T_0 mixing rate. This is a novel phenomenon that can occur in radical pair reactions in crystals, viscous media, micelles, surfaces and the like.

GENERAL THEORY

Spin Hamiltonian and Stochastic Liouville Equation

Our goal in this section is to predict the magnetic field and orientation dependence of the quantum yield of products of radical pair reactions in the solid state. Similar approaches are used to calculate other observables, such as radical pair kinetics, nuclear and electron spin polarization, RYDMR effects, and isotope fractionation. We adopt the reaction scheme in RCs (Figure 3B), which is representative of radical pair reactions. The variables

are the radical pair recombination rate constants, k_S and k_T, and the parameters of a spin Hamiltonian for the radical pair (4, 50):

$$\mathcal{H} = \mathbf{S}_1 \cdot (\mathcal{g}_1 \cdot \mathbf{H}\beta_e + \sum_i \mathcal{A}_{il} \cdot \mathbf{I}_{il}) + \mathbf{S}_2 \cdot (\mathcal{g}_2 \cdot \mathbf{H}\beta_e + \sum_i \mathcal{A}_{i2} \cdot \mathbf{I}_{i2})$$
$$+ J\mathbf{S}_1 \cdot \mathbf{S}_2 + \mathbf{S}_1 \cdot \mathcal{D} \cdot \mathbf{S}_2 + \sum_{i,j} \gamma_{ij}\hbar \mathbf{I}_{ij} \cdot \mathbf{H} + \sum_{i,j} \mathbf{I}_{ij} \cdot \mathcal{P}_{ij} \cdot \mathbf{I}_{ij}, \quad 1.$$

where $\mathbf{S}_1$ and $\mathbf{S}_2$ and $\mathcal{g}_1$ and $\mathcal{g}_2$ are the angular momentum operators and g-tensors for unpaired electrons on radicals 1 (P^+) and 2 (I^-), respectively. $\mathcal{A}_{ij}$, $\mathcal{P}_{ij}$, $\mathbf{I}_{ij}$, and γ_{ij} are the hyperfine tensor, quadrupole tensor, angular momentum operator, and magnetogyric ratio for the ith nucleus on the jth radical, respectively. J and $\mathcal{D}$ are, respectively, the isotropic exchange coupling constant and the dipole-dipole tensor for the unpaired electron on P^+ interacting with the unpaired electron on I^-. β_e is the Bohr magneton.

Triplet yields are calculated using a density operator approach, as introduced by Schulten and Haberkorn and their co-workers. The Stochastic Liouville equation describes the time evolution of the density operator, $\rho(t)$, under the influence of the spin Hamiltonian and the recombination reactions (Figure 3B) (5, 42, 43):

$$d\rho(t)/dt = \frac{-i}{\hbar}[\mathcal{H}, \rho(t)]_- - \frac{1}{2}k_S[P^S, \rho(t)]_+ - \frac{1}{2}k_T[P^T, \rho(t)]_+, \quad 2.$$

where P^S and P^T are the singlet and triplet projection operators, respectively. The first term on the right-hand side describes the coherent evolution of the system among the singlet and triplet states. The second two terms introduce decay in the singlet and triplet parts of the density operator due to radical ion pair recombination. The spin Hamiltonian is not the complete Hamiltonian, and these additional terms are added to account for those processes that do not manifest coherence and are assumed to be adequately described by first-order rates. One half of the anticommutator of the singlet projection operator and the density operator,

$$(1/2)[P^S, \rho(t)]_+ = (1/2)[P^S\rho(t) + \rho(t)P^S],$$

projects out the probability that the radical pair is in the singlet state at time t. Multiplication of this singlet "concentration" by the first-order rate constant k_S gives the rate at which radical pairs are collapsing by the singlet pathway. Relaxation terms for either the electrons or nuclei have not been included because the electron and nuclear spins are not expected to undergo relaxation during the lifetime of the radical pair (about 10 ns). This approximation would not be valid for much longer-lived radical pairs, but Eq. 2 could be modified as in Redfield theory (51) or Freed's elegant treatment of CIDEP (52).

The triplet yield can be obtained from $\rho(t)$ or more simply from

$$\bar{\rho} \equiv \int_0^\infty \rho(t)\, dt,$$

as

$$\Phi_T = \int_0^\infty Tr[k_T P^T \rho(t)]\, dt = k_T Tr(P^T \bar{\rho}). \quad 3.$$

$\bar{\rho}$ can be obtained by integrating Eq. 2 over all time and solving the resulting algebraic equation

$$B\bar{\rho} + \bar{\rho}B^\dagger = \rho(0), \quad \text{where} \quad B \equiv \frac{i}{\hbar}\mathscr{H} + \frac{1}{2}k_S P^S + \frac{1}{2}k_T P^T. \quad 4.$$

The initial condition is that the radical pair starts in the singlet state:

$$\rho(0) = \frac{1}{N} P^S$$

where N is the total number of nuclear states.

We discuss calculations of the quantum yield for three cases:

1. a high-field analytical solution developed by us (45);
2. a zero-field one-proton analytical solution developed by Haberkorn et al (43);
3. numerical solutions for zero and low fields developed by Schulten et al (42).

High Field

High field is the region for which the electron Zeeman interaction is much greater than the electron-electron dipolar, exchange, or hyperfine interactions. This occurs in Q-depleted RCs for fields greater than about 1000 G. We can neglect terms of the form $I_x S_x$ and $I_y S_y$ that induce transitions between the set of states $\{S, T_0\}$ and the set $\{T_+, T_-\}$, because the large Zeeman energy difference between these two sets of states prevents transitions between them. In addition we make the specialized approximations that the g-factor anisotropies are small and neglect the nuclear Zeeman and nuclear quadrupole interactions. These approximations are very reasonable for P^+ and I^- (49). Neither the nuclear Zeeman nor the nuclear quadrupole interactions couple singlet and triplet electron spin states directly. They can, however, modify the effective hyperfine coupling by mixing nuclear states; this approximation must be considered on a case-by-case basis for other radical pair reactions.

With these approximations, the Hamiltonian for the kth nuclear state, $\mathscr{H}'_k$, takes the following form at high field:

$$\mathscr{H}'_k = \left[g\beta_e H + \sum_i A_{i2}(\beta,\gamma) m^k_{i2} \right] S_z + (3/4) D_{zz}(\beta,\gamma) S_z^2 + (1/2)\Delta E(\beta,\gamma)\mathbf{S}^2 + \hbar\omega_k(H,\beta,\gamma) S_{1z}, \quad 5.$$

where

$$\Delta E(\beta,\gamma) = J - (1/2) D_{zz}(\beta,\gamma),$$

$$\omega_k(H,\beta,\gamma) = (1/\hbar)\left[\Delta g(\beta,\gamma)\beta_e H + \sum_i A_{i1}(\beta,\gamma) m^k_{i1} - \sum_i A_{i2}(\beta,\gamma) m^k_{i2}\right],$$

$$\mathbf{S} = \mathbf{S}_1 + \mathbf{S}_2, \quad A_{ij}(\beta,\gamma) = |\hat{\mathbf{z}} \cdot \mathscr{A}_{ij}|, \quad g = (\mathscr{g}_2)_{zz},$$

$$\Delta g(\beta,\gamma) = (\mathscr{g}_1 - \mathscr{g}_2)_{zz} = \Delta g_{iso} + \Delta g_{ax}[3(\hat{\mathbf{z}} \cdot \hat{\mathbf{z}}_g)^2 - 1] - \Delta g_{rh}[(\hat{\mathbf{z}} \cdot \hat{\mathbf{x}}_g)^2 - (\hat{\mathbf{z}} \cdot \hat{\mathbf{y}}_g)^2],$$

$$D_{zz}(\beta,\gamma) = (\mathscr{D})_{zz} = 2D[(\hat{\mathbf{z}} \cdot \hat{\mathbf{z}}_D)^2 - 1/3] - 2E[(\hat{\mathbf{z}} \cdot \hat{\mathbf{x}}_D)^2 - (\hat{\mathbf{z}} \cdot \hat{\mathbf{y}}_D)^2].$$

Here, m^k_{ij} is the quantum number of angular momentum in the direction of the effective hyperfine field, $\hat{\mathbf{z}} \cdot \mathscr{A}_{ij}$, for nucleus i on radical j in the kth nuclear spin state, the standard zero field parameters D and E have been used, and the difference g-tensor principal values have been parameterized as isotropic (Δg_{iso}), axial (Δg_{ax}) and nonaxial (Δg_{rh}) components.

The following notation has been used. The laboratory-fixed axis system is designated by the unit vectors: $\hat{\mathbf{x}}$, $\hat{\mathbf{y}}$, $\hat{\mathbf{z}}$, with the magnetic field in the $\hat{\mathbf{z}}$ direction. The sample-fixed axis system is designated by $\hat{\mathbf{a}}$, $\hat{\mathbf{b}}$, and $\hat{\mathbf{c}}$. The sample-fixed axis system is related to the laboratory axis system by the Euler angles α, β, and γ (53). The principal axes of the tensors describing the anisotropic magnetic interactions are $\hat{\mathbf{x}}_i$, $\hat{\mathbf{y}}_i$, and $\hat{\mathbf{z}}_i$, where i is D for the electron dipole-electron dipole tensor, A for nuclear hyperfine tensors, P for nuclear quadrupole tensors, or g for the *difference* g-tensor between the radicals in the pair. The orientation of the principal axis system of each anisotropic interaction with respect to the sample-fixed axis system is described by the three Euler angles: α_i, β_i, γ_i. For simplicity, we adopt the following truncated subscript notation: The components of a tensor in its principal axis system are denoted with single subscripts, as in A_x, A_y, and A_z for the principal values of the hyperfine tensor, and the components in the laboratory axis system by the standard double subscript, as in A_{zz}.

In the above high field Hamiltonian, the mixing of S and T_0 is determined by the energy splitting, $\Delta E(\beta,\gamma)$, and by the coupling constant, $\omega_k(H,\beta,\gamma)$, which is the frequency of S-T_0 mixing in the absence of an energy splitting.

Equation 3 can then be solved analytically using the method introduced by Haberkorn (43). The "single orientation" yield, $\Phi_T(H,\beta,\gamma)$, is the yield averaged over nuclear states

$$\Phi_T(H,\beta,\gamma) = \left(\frac{k_T}{k_S+k_T}\right)\frac{1}{N}\sum_{k=1}^{N}\frac{1}{1+[\kappa(\beta,\gamma)/\omega_k(H,\beta,\gamma)]^2}, \qquad 6.$$

where

$$\kappa^2(\beta,\gamma) = k_S k_T\{1+[2\Delta E(\beta,\gamma)/\hbar(k_S+k_T)]^2\}.$$

The nuclear averaging warrants two comments. First, it assumes equal weights for each nuclear state, essentially the Boltzmann distribution at normal temperatures. Although one can envision very interesting situations in which this assumption might break down due to the presence of nuclear spin polarization, there are no cases at the present time. Second, averaging over independent nuclear states is a rigorous approach in the high field limit, contrary to a recent, incorrect assertion (43a).

As the number of nuclear states is generally large in organic radicals, the summation over discrete nuclear states in Eq. 6 may be replaced with an integral over a Gaussian distribution of hyperfine energies. This leads to a Gaussian distribution in the coupling contants, $\omega(H,\beta,\gamma)$, centered at $\Delta g(\beta,\gamma)\beta_e H/\hbar$ with second moment, $[A(\beta,\gamma)/2\hbar]^2$. For the case of RCs, we consider only an axial hyperfine energy width; thus

$$A^2(\beta,\gamma) = A_{iso}^2 + A_{ax}^2[(\hat{\mathbf{z}}\cdot\hat{\mathbf{z}}_A)^2 - 1/3]. \qquad 7.$$

Equation 6 for the quantum yield can now be expressed in terms of two reduced parameters, σ and Δ, and the infinite field yield, $k_T/(k_S+k_T)$:

$$\Phi_T(H,\beta,\gamma) = \left(\frac{k_T}{k_S+k_T}\right)\frac{1}{\sqrt{2\pi}}\int_{-\infty}^{\infty}\frac{(\sigma y+\Delta)^2}{(\sigma y+\Delta)^2+1}e^{-(1/2)y^2}\,dy, \qquad 8.$$

where

$$\sigma = \frac{A(\beta,\gamma)}{2\hbar\kappa(\beta,\gamma)} \quad \text{and} \quad \Delta = \frac{\Delta g(\beta,\gamma)\beta_e H}{\hbar\kappa(\beta,\gamma)}.$$

For a radical pair reaction in a single crystal this last result could be compared directly with experiment. For less ordered systems, some type of spatial averaging is necessary. Here we translate the "single orientation" yield into the experimental "observed yield," specialized for the particular method used to measure the yield anisotropy in RCs. In order to observe an anisotropic yield in an isotropic sample of RCs, we use an anisotropic detector, in this case linearly polarized light at 870 nm, which detects an anisotropic depletion of *P*. Thus, we perform a weighted average over

orientations for the electric unit vector, $\hat{\mathbf{E}}$, of a linearly polarized probe beam at the angle η to the field direction:

$$\Phi_T^{obs}(H,\eta) = (3/8\pi^2)\int_0^{2\pi}\int_0^{\pi}\int_0^{2\pi}[\hat{\mathbf{E}}(\eta)\cdot\hat{\boldsymbol{\mu}}(\alpha,\beta)]^2\Phi_T(H,\beta,\gamma)\,d\alpha \times \sin\beta\,d\beta\,d\gamma. \quad 9.$$

The c-axis is defined to lie along the transition dipole moment direction, $\hat{\boldsymbol{\mu}}$, used to detect the quantum yield anisotropy. The isotropically averaged quantum yield, $\Phi_T^{av}(H)$, is

$$\Phi_T^{av}(H) = (1/3)[\Phi_T^{obs}(H,0^0)+2\Phi_T^{obs}(H,90^\circ)], \quad 10.$$

and the "quantum yield anisotropy," is

$$a(H) = \frac{\Phi_T^{obs}(H,0^\circ)-\Phi_T^{obs}(H,90^\circ)}{\Phi_T^{obs}(H,0^\circ)+2\Phi_T^{obs}(H,90^\circ)}. \quad 11.$$

Structural information is contained in the Euler angles α_i, β_i, and γ_i, which relate the principal axes of the various interactions to each other and to the transition dipole moment.

Low Field

At low magnetic field, nuclear states are coupled and the treatment above is not applicable. A series of approaches of increasing complexity, none without shortcomings, has been applied to this problem. For the case of only one proton coupled to one of the electrons and in the absence of electron-electron dipolar coupling, an analytical solution at zero field has been provided by Haberkorn & Michel-Beyerle (43):

$$\Phi_T(H=0) = 3(A/\hbar)^2k_T(k_S+k_T)/\{[3(A/\hbar)^2+4k_Sk_T](k_S+k_T)^2 + 16k_Sk_T(J-A/2)^2/\hbar^2\}, \quad 12.$$

where A is the isotropic hyperfine coupling constant for the one proton. Consideration of nonzero fields or more magnetic hyperfine interactions is much more difficult, and no analytical expression is available at this time.

A numerical treatment has been introduced by Schulten et al (42) to deal with more than one proton at arbitrary field ($\Delta g = 0$); most calculations were for a two-proton model. We have modified this treatment for inclusion of the dipolar interaction (47). Equation 4 was solved numerically using the Hamiltonian of Eq. 1 with isotropic g-factors, the isotropic exchange interaction, an anisotropic dipolar interaction, and one isotropic proton hyperfine interaction on each radical (a two proton model): $(A_{P+})/g_e\beta_e = -9.5$ G and $(A_{I-})/g_e\beta_e = 13$ G, which are consistent with the known EPR

data for $P^{\ddagger}$ (54) and $I^{\cdot-}$ (55). The negative sign for $A_{P^{\ddagger}}$ was used to avoid a physically unreasonable model in which the singlet states are only coupled to triplet states with small or negative hyperfine energies, but not to triplet states with large positive hyperfine energies.

A further extension of this approach has recently been presented by Tang & Norris (56). As described by these investigators, a Gaussian distribution of hyperfine interactions for each member of the radical pair was used, by doing calculations for seven points ranging from $-2^{1/2}\sigma_1$ (and $-2^{1/2}\sigma_2$) to $2^{1/2}\sigma_1$ ($2^{1/2}\sigma_2$) for the Gaussian distribution of A_1 (and A_2), respectively, where σ_1^2 (about 20 G^2) and σ_2^2 (about 64 G^2) are the second moments for the two distributions ($1 = P^{\ddagger}$, $2 = I^{\cdot-}$). This method would emphasize small effective hyperfine fields. As the total hyperfine field and not just the z-component is effective in generating triplets at low field, this center-weighted distribution for the coupling constants A_1 and A_2 may not be appropriate. As pointed out in a semiclassical analysis of this problem by Schulten & Wolynes (12), a three-dimensional Gaussian distribution of hyperfine fields is an appropriate model, particularly for dealing with a large number of nuclei.

The important new idea introduced by us (47) and by Tang & Norris (56) is that the anisotropic dipolar interaction can have a major effect on the isotropic quantum yield at low field in the solid state. A complication is that the particular approximation used to model the hyperfine interaction will affect the magnitudes of parameters obtained in fitting the data.

Other States and Interactions

The scheme in Figure 3B has been embellished in two related ways in recent treatments. The first modification includes the activated back reaction from $^1P^{\ddagger}I^{\cdot-}$ to ^1PI with rate constant $k_{S'}$ (43a). This introduces a further singlet decay channel and delayed fluorescence as an additional observable. Further, the inclusion of ^1PI in the spin dynamics of the radical pair provides a dephasing mechanism that can slow S-T mixing and destroy coherence.

A related modification to the scheme by Haberkorn and co-workers (57), whose consequences have been more rigorously explored, introduces an intermediate electron acceptor. That is, the species I is considered to be comprised of two species, B and H, and the initial reaction sequence becomes:

$$^1PBH \rightarrow P^{\ddagger}B^{\cdot-}H \underset{k_D}{\overset{k_C}{\rightleftarrows}} P^{\ddagger}BH^{\cdot-}$$

The electron exchange interaction in the state $P^{\ddagger}B^{\cdot-}H$ is taken to be much larger than in the state $P^{\ddagger}BH^{\cdot-}$ and acts to dephase singlet and triplet

radical pairs. Haberkorn et al (57) have shown that triplet quantum yields in this modified scheme would be reduced from those calculated with the methods discussed above by the factor $k_C/(k_C+k_S)$, and that electron hopping leads to an additional phase relaxation term in the Stochastic Liouville equation (Eq. 2).[1] It is difficult to demonstrate the presence of such an intermediate from relative triplet yield measurements, because the new relaxation term leads to a level broadening effect which affects the triplet yield very much like the dipolar interaction or large values of the decay rate constant, k_T (see *Low Field Isotropic Yield* section below). If k_C is not much greater than k_S, a discrepancy between calculated and measured absolute yields may signal the presence of the intermediate. Though shown to be rigorous for the calculation of relative triplet yields, the use of Eq. 2 with effective parameters is valid for the calculation of time dependent concentrations only if k_C is very large.

Another interaction is possible in RCs containing Q_A^-. Spin exchange between I^- and Q_A^- introduces another mechanism of S-T mixing, as the phase of the spin on Q_A^- is uncorrelated with those in the radical pair. This effect is complex because the spin on Q_A^- is also strongly coupled to a nearby high-spin Fe(II) in the RC. We have shown that spin exchange between I^- and Q_A^- Fe(II) can lead to a strongly field dependent contribution to the S-T mixing (47) because the Zeeman interactions of the two spins are known to be very different (58). An earlier theoretical consideration neglected the differences in Zeeman interaction, which led to the conclusion that spin exchange would provide a field-independent S-T mixing mechanism (42).

Other Observables

Although this review focuses on the effects of magnetic fields on the triplet quantum yield, several other observables supplement the field effect data and can be used to fix parameters with greater certainty. A first example is the radical pair decay kinetics, which can be obtained by solving Eq. 2 for all times. Tang & Norris (56) have shown that with $k_T > k_S$, the radical pair decay is nearly exponential, a result that encourages the use of a simple expression introduced earlier by Haberkorn et al (43):

$$\tau = \int_0^\infty \mathrm{Tr}(\rho)\, dt = (1-\Phi_T)/k_S + \Phi_T/k_T. \qquad 13.$$

With $k_S > k_T$, the decay appears biexponential with decay rates near k_S and k_T.

[1] The parameters k_S, k_T, and J should be replaced by k_S^{eff}, k_T^{eff}, and J^{eff} in Eq. 2, and the term $-[(k_2^{eff}-(1/2)(k_S^{eff}+k_T^{eff})]\,[P^T\rho P^S + P^S\rho P^T]$ added.

A second observable is the delayed fluorescence of the precursor excited state, ^1P, mentioned above that is produced by back reaction from the singlet radical pair. This fluorescence should decay with the same kinetics as the singlet radical pair, because the forward electron transfer reaction is fast. Thus, it should decay in parallel with the total radical pair concentration at short time, but may deviate at longer time if $k_S > k_T$.

A third observable is the RYDMR effect. The theoretical approach to calculating this effect and the kind of information obtained are similar to those for the magnetic field effects (58a,b). At resonant magnetic fields, microwaves cause transitions between triplet radical pair levels, perturbing the spin dynamics in the radical pair and thus affecting the triplet yield. The RYDMR linewidth and intensity as a function of microwave power are new observables, which provide an additional and, in certain cases, more direct way of determining magnetic and kinetic parameters of the radical pair.

EXPERIMENTAL RESULTS

Isotropic and Anisotropic Magnetic Field Effects in RCs

The absorption of P at 870 nm was selectively probed with light polarized either parallel or perpendicular to the magnetic field after pulsed excitation. The absorption was probed after P^+I^- had completely decayed, but before ^3P had decayed to any significant extent. Thus, an anisotropic distribution of RCs was selected for detection. The details of the measurements of the anisotropic field effects and absolute triplet quantum yields at zero field are presented elsewhere (49, 59). Quinone-depleted RCs were suspended in ordinary aqueous buffers for measurements of isotropic quantum yields or viscous buffer (containing glycerol) for measurements of anisotropic quantum yields (49).

Figure 5 shows the triplet quantum yield for Q-depleted RCs suspended in buffer at 293 K between 0 and 50 kG. There is an initial rapid drop-off in the quantum yield of triplets when the field is applied (0–2 kG), followed by a rise in the yield on going to higher magnetic fields. On going from 2 to 50 kG, the quantum yield increases by about 136%. At fields less than 10 kG, the yield increase is quadratic in field, but at higher magnetic fields there is evidence for the predicted leveling off of the yield. The relative quantum yield for magnetic fields between 0 and 500 G is shown in the *inset* to Figure 5. The quantum yield decreases monotonically on application of a field, with a $B_{1/2}$ value of 42 G. $\Phi_T(H)$ is approximately constant between 0 and 10 G, and equals 0.22 (59).

Figure 6A shows the results of a set of experiments on RCs suspended in a

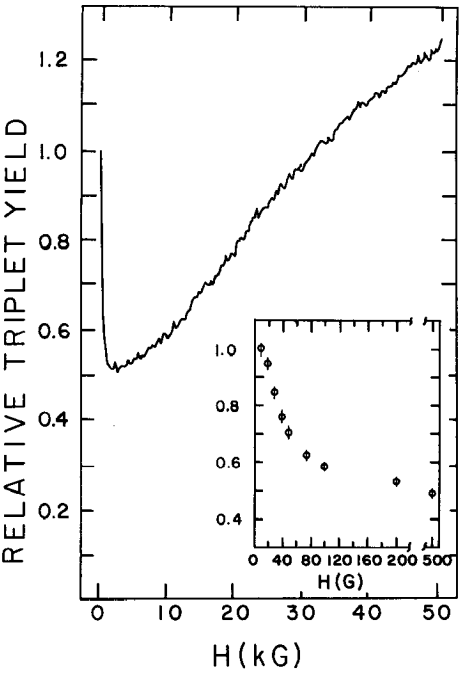

Figure 5 Relative yield $I(H, 90°)$ in Q-depleted RCs at 293 K between 0 and 50 kG. *Inset*: expansion of the low field region from 0 to 500 G. For the latter, error bars are the standard deviation determined from five experiments on two samples; field strengths are accurate to within 2 G.

viscous solvent with the observation light polarized either parallel ($\eta_0 = 0°$) or perpendicular ($\eta_0 = 90°$) to the magnetic field. The quantum yield anisotropy, $a(H)$ (Eq. 10) is plotted in Figure 6B. Absorption at 870 nm in RCs is due almost entirely to P and the transition is strongly polarized. Thus, as a consequence of the anisotropic chemistry, the sample becomes transiently dichroic. Note that both the sign and magnitude of $a(H)$ may be completely different if detected at another wavelength, as the transition moment probed at another wavelength may point in an entirely different direction within the RC. RCs suspended in nonviscous buffer undergo rotational diffusion in the 3 μs delay between the creation of the triplet state and its detection. This rotation completely destroys the dichroism, as is seen in the control experiment (Figure 6B, *triangles*). It should be noted that even in nonviscous buffers, magnetic field effect experiments with much greater time resolution (on the time scale of the rotational correlation time of the RC, about 20 ns) may contain artifacts due to anisotropic quantum yields. This problem would be particularly acute for time-resolved measurements, because the artifact would decay in time. This may be of no consequence for

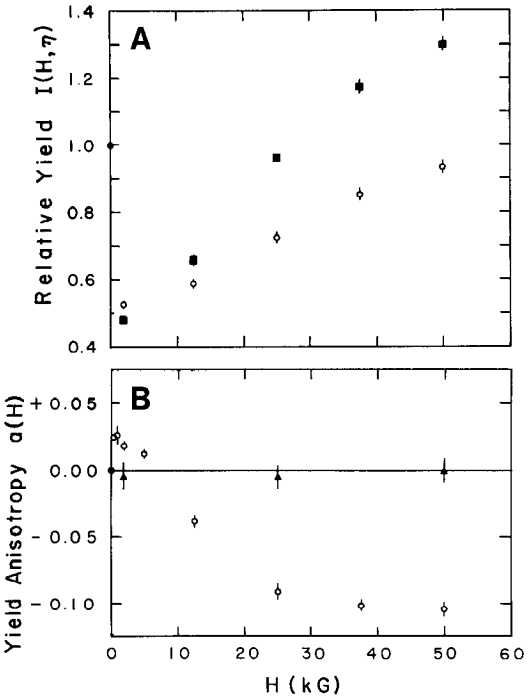

Figure 6 (A) The relative quantum yield, $I(H, \eta)$, as a function of magnetic field strength for Q-depleted RCs at 293 K in viscous glycerol/buffer ($\eta = 0°$: *circles*; $\eta = 90°$: *squares*). (B) The quantum yield anisotropy, $a(H)$, in viscous glycerol/buffer (*circles*) and in nonviscous buffer (*triangles*).

observation wavelengths and fields where $a(H)$ is very small, but it can be very important under other circumstances.

The extraordinary observation in Figure 6B that $a(H)$ is positive at low fields and negative at high fields indicates that there are two or more anisotropic magnetic interactions contributing to the yield anisotropy detected at 870 nm. This "chemically induced dichroism" is not to be confused with photoselection, whereby a partially oriented (cosine-squared) population of RCs can be created by excitation of a pure electronic transition using linearly polarized light. We have shown elsewhere (49) that the effect of varying the angle, η_e, between the electric vector of the excitation pulse and the magnetic field is much smaller than the effect of varying η_0. This result, and the fact that the sample is not oriented by the field, show that the sample is effectively isotropically excited.

Other Experiments

Measurements by Parson and co-workers (39) of the radical pair lifetime

and fluorescence as a function of temperature, field, and isotopic substitution are complex and interesting. $\Phi_T(H = 0)$ is about 0.14 at room temperature in both protonated and deuterated Q_A^--containing RCs. The yield decreases by about 0.05 in both samples at 650 G. The radical pair decay rate shows a substantial effect of field at room temperature. It is $9 \times 10^7\ s^{-1}$ at zero field, but drops to $7 \times 10^7\ s^{-1}$ at 650 G. Deuteration affects the decay rate, decreasing the rate at all temperatures and both fields by about 25%. At room temperature, depletion of quinone in protonated RCs has no effect on the decay rate and increases the triplet yield by a factor of two. The fluorescence at zero field from both Q-depleted and Q_A^- RCs increases from room temperature down to 200 K, then decreases about two-fold on lowering to 100 K; it is independent of temperature if Q_A is not reduced. Application of a 650 G field increases the fluorescence by only 1.6% at room temperature in Q_A^--containing RCs. The fluorescence lifetime in Q_A^- RCs showed an instrument-limited (6 ns fwhm) fast component and a slower component of $1.7 \times 10^8\ s^{-1}$.

Ogrodnik et al (60) reported the relative concentrations of P^+I^-, ^3P and P in freshly Q-depleted RCs 3, 5, 7 and 15 ns after a saturating 1.5 ns excitation pulse. They also report the low field dependence of the ^3P concentration at these times. At zero field, the ground state concentration initially rises faster than the triplet state, though the final triplet yield appears to be near 50%. At 3 ns, the triplet concentration at 400 G is 33% of its value at zero field, but at 15 ns it is 44% of the zero field value. $B_{1/2}$ decreases from 80 G at 3 ns to 33 G at 15 ns. The Q-depletion procedure and time between depletion and measurement can affect the magnetic field effects. It is not yet clear whether RCs freshly depleted of quinones are more or less representative of native RCs.

The RYDMR linewidth for Q-depleted RCs at about 3000 G is 25–30 G with relatively low power (13f). The maximum RYDMR intensity is an 8% increase in the triplet yield when 2000 W of microwave power is applied (H_1 estimated to be 20 G). As the power is increased further, the signal decreases, becomes negative, and broadens.

Data for quinone-containing RCs show a very wide variation in different laboratories. In part this is due to photochemical changes that occur during the experiment (59); however, the precise nature of these changes remains obscure and further discussion of the magnetic field effects is not warranted at this time. Magnetic field effects have been observed in membrane preparations, whole cells, and large, subchloroplast preparations (43a). As a result of the added complications of energy migration, trapping, and activated detrapping, we feel it is premature to undertake a quantitative analysis based on schemes such as Figure 3B.

EFFECTS OF PARAMETERS AND COMPARISON WITH EXPERIMENTS

High Field Isotropic Yield

Figure 7 shows the magnetic field dependence of the calculated yield between 0 and 50 kG for various values of the kinetic and magnetic parameters, omitting all anisotropic interactions. From the measured EPR linewidths of $P^{\ddagger}$ [9.5 G (54)] and $I^{\cdot}$ [13 G (55)], $(A_{iso}/g_e\beta_e)^2 = (9.5)^2 + (13)^2 = (16\ G)^2$; see Eq. 7. A large value of Δg leads to a rapid initial rise in Φ_T with field above 1 kG and an early leveling off. Large values of k_S or J serve to decrease Φ_T, without substantially changing the absolute amount of modulation of the yield by the magnetic field. The effect of increasing values of k_T is more complicated: the 1 kG yields at first increase with increasing values of k_T, reach a maximum, and then decrease as k_T becomes large.

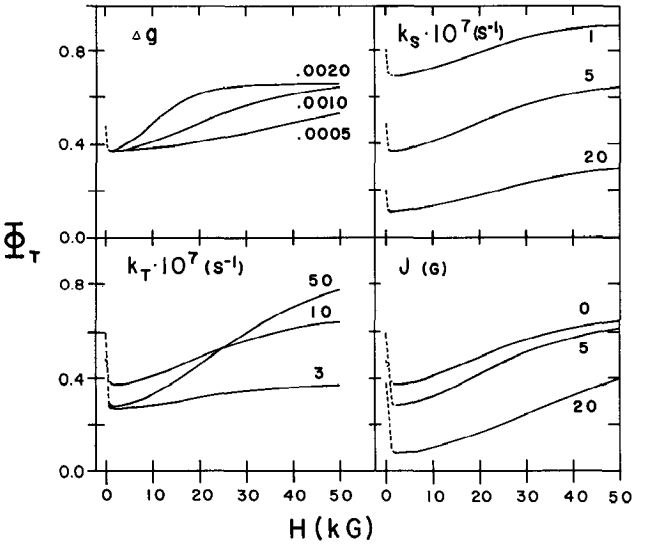

Figure 7 The dependence of the isotropic high-field yield on the values of k_S, k_T, Δg, and J. The values of D and E were taken to be zero, and Δg and the hyperfine interactions were taken to be isotropic. In each panel, one parameter is varied while the others are kept at the following values:

$A_{iso}/g_e\beta_e = 16\ G$; $k_S = 5 \times 10^7\ s^{-1}$; $k_T = 1 \times 10^8\ s^{-1}$;

$\Delta g = 0.0010$; $J = 0\ G$.

The yields at zero field were calculated with the one proton model (Eq. 12), and at high fields with Eq. 8.

Whenever k_T becomes much larger than ω, the triplet yield decreases with larger values of k_T. This may be viewed as due to lifetime broadening of the triplet levels (43). At 50 kG the larger values of k_T in Figure 7 continue to give larger triplet yields because ω is large due to the Δg effect. The parameters k_S, k_T, J, and Δg all scale linearly with the hyperfine interactions. Thus if the hyperfine interactions, k_S, k_T, J, and Δg are all doubled, none of the high-field curves in Figure 7 changes.

High Field Anisotropic Yield

In this section physically reasonable values for the magnitude of each anisotropic magnetic interaction in the radical pair $P^{\ddagger}I^{\ddagger}$ are used to illustrate the effects that each of these interactions would have in the absence of the others. A much more detailed analysis of the particular values is presented in Ref. (49). As there are many possible permutations of the parameters in this problem, only a selected set is discussed below to illustrate some of the interesting situations that can arise. Very little is known at this time about the anisotropic magnetic properties of $P^{\ddagger}$ and $I^{\ddagger}$. This may not be the case in other systems, so more definitive structural data about radical pair intermediates could be extracted from quantum yield anisotropy data.

NUCLEAR HYPERFINE INTERACTIONS Consideration of the nature of $P^{\ddagger}$ and $I^{\ddagger}$ shows that the largest anisotropic hyperfine interactions probably are associated with two of the central ^{14}N on $I^{\ddagger}$. As shown in (49), one can approximate this with an axial hyperfine interaction, A_{ax} (see Eq. 7):

$$(A_{ax}/g_e\beta_e)^2 = 2(4/3)I_N(I_N+1)[(5.7)^2-(0.6)^2] = (13.1\ \text{G})^2.$$

Figure 8A shows the expected field dependence of the yield anisotropy due to anisotropic hyperfine interactions for various orientations of the hyperfine principal axis, ignoring the other anisotropic interactions. The small negative anisotropies at high field are due to saturation of the triplet yield at large values of the ω distribution.

ELECTRON-ELECTRON DIPOLAR INTERACTION Figure 8B shows the yield anisotropy due to only the electron-electron dipolar interaction (the hyperfine and g tensors are taken to be isotropic). This figure also demonstrates the extreme sensitivity of the anisotropy to the strength of the exchange interaction J. The values of α_D, β_D, and γ_D chosen in Figure 8B place $\hat{\boldsymbol{\mu}}_{870}$ along $\hat{\mathbf{z}}_D$, giving the maximum effect obtainable. If the $S\text{-}T_0$ energy splitting, ΔE, is larger with $\hat{\mathbf{z}}_D \| \mathbf{H}$ than with $\hat{\mathbf{z}}_D \perp \mathbf{H}$, then the anisotropy will be negative. The addition of J to the problem can either accentuate this effect, decrease it, or even reverse its sign. Another interesting aspect of the dipolar-induced anisotropy is the prediction of

anisotropies greater than 2/5 or less than $-1/5$, the limits for a normal fluorescence or phosphoresence polarization experiment (61). When the anisotropic distribution is created by absorption of polarized light, as in a normal photoselection experiment, the distribution of excited states depends on the square of the cosine between the absorbing transition moment and the electric vector of the exciting light. By contrast, the anisotropic quantum yield is created by anisotropic chemistry, not by photoselection, and may have a more sharply peaked distribution than cosine squared, giving rise to anisotropies outside the normal range.

DIFFERENCE g TENSOR Organic radicals have only very minor g-tensor anisotropies, with principal values deviating from the g-factor of the free electron, 2.0023, by amounts on the order of 10^{-3} (50). Δg_{ax} and Δg_{rh} are expected to be of this order of magnitude. As an example, the effect of $\Delta g_{ax} < 0$ with $\Delta g_{rh} = 0$, is shown in Figure 8C.

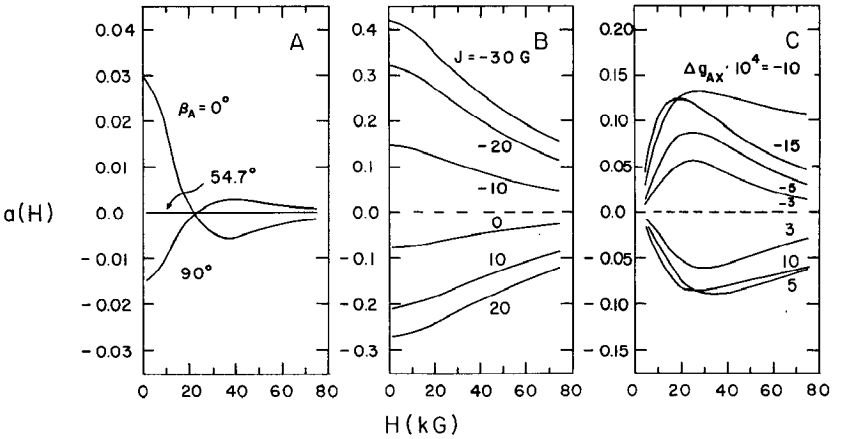

Figure 8 The effects of various parameters on the yield anisotropy, $a(H)$. The likely largest possible variations for a radical pair of the type in RCs are illustrated. (Note the large differences in vertical scales.) In each panel, one parameter is varied while the others are kept at the following values:

$k_S = 1 \times 10^8\ s^{-1}, k_T = 1 \times 10^8\ s^{-1}$; $A_{iso}/g_e\beta_e = 16$ G, $A_{ax} = 0$;

$J = D = E = 0$; $\Delta g_{iso} = -9 \times 10^4, \Delta g_{ax} = 0, \Delta g_{rh} = 0$.

(A) The effect of the anisotropy of the ^{14}N hyperfine interactions in I^-, as a function of the angle, β_A, between the hyperfine axis and $\hat{\mu}_{870}$. $A_{ax}/g_e\beta_e = 13.1$ G. (B) The effect of the electron-electron dipolar interaction, illustrating the enormous effect of the electron exchange interaction:

$D/g_e\beta_e = -45$ G, $E/g_e\beta_e = 15$ G, $\beta_D = 0°$.

(C) The effect of the g-tensor anisotropy. The yield anisotropy, $a(H)$, due to Δg_{ax}. $\beta_g = 0°$.

COMPARISON WITH EXPERIMENT Figure 9 shows both some calculated curves and the experimental data points for $\Phi_T^{av}(H)$ and $a(H)$ between 1 and 50 kG for the parameters listed in the caption. The parameters were obtained as follows: J, D, and E are those values suggested by an analysis of the data at low field (see below). The experimental values of Φ_T^{av}(1 kG) and Φ_T^{av}(50 kG) determine k_S and k_T. The curvature of $\Phi_T^{av}(H)$ between 1 and 50 kG determines Δg_{iso}. From Figure 8 it is clear that either dipolar or hyperfine anisotropy is sufficient to account for the anisotropy at 1 kG, so values for α_D, β_D, γ_D, α_A, and β_A were arbitrarily chosen to give the correct value of a(1 kG), which is quite small. Future epr experiments on oriented $P^{\dagger}$ and $I^{\bar{\cdot}}$ and RYDMR experiments on $P^{\dagger}I^{\bar{\cdot}}$ should determine which interaction is most important at this particular wavelength.

Most of the anisotropy at 37.5 and 50 kG is due to the g factor anisotropy. If the anisotropy of +0.026 at 1 kG is due to the hyperfine interactions, their contribution to the anisotropy should have decreased to about −0.005 by 30 kG (cf Figure 8A). Alternatively, if the anisotropy at 1 kG is due to the electron-electron dipolar interaction, its contribution to the anisotropy would decrease to less than 0.015 by 30 kG (cf Figure 8B). Thus the anisotropy due to Δg alone between 37.5 kG and 50 kG must be about −0.10 or more. Using either Δg_{ax} or Δg_{rh}, this very negative value of the anisotropy can be reproduced only when $\hat{\mu}_{870}$ is parallel to a principal axis of Δg and with the principal value of Δg along that axis close to zero. Note that for the particular values of k_S, k_T, and Δg_{iso} chosen in Figure 9, the largest negative anisotropy at 40 kG for any value of Δg_{ax} is approximately the experimental value, a(40 kG) = −0.10.

Many RC structures can be imagined that would make the value of Δg be zero along $\hat{\mu}_{870}$. Though it is difficult to turn the results of this experiment into structural knowledge of the RC at the present time, the reverse process would be most interesting. Should a crystal structure for RCs ultimately become available, the expected value of the anisotropy could be calculated with some condifence. The experimental anisotropy could then be used, for example, to decide which among the various chromophores in the RC acts as the intermediate acceptor I.

Low Field Isotropic Yield

The effects of k_S, k_T, and J on the low field yield have been considered previously by Schulten et al (42) and Haberkorn et al (43, 62). They showed that the triplet radical pair levels are broadened by hyperfine interactions and that both the singlet and triplet levels are lifetime broadened. The value of $B_{1/2}$, in the absence of dipolar coupling, is then determined by whichever is largest: $\hbar k_S/g_e\beta_e$, $\hbar k_T/g_e\beta_e$, or the hyperfine interaction energy expressed in Gauss. For $J = D = E = 0$, reasonable fits to a $B_{1/2}$ of 42 G can be

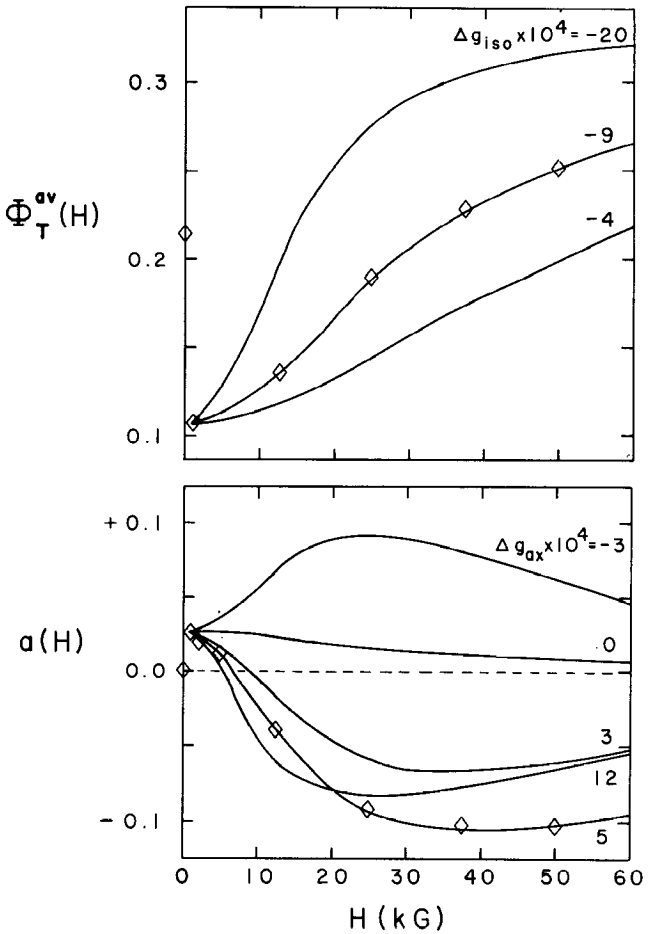

Figure 9 (A) Calculated (——) and experimental (*diamonds*) average quantum yields, $\Phi_T^{av}(H)$, as a function of magnetic field strength. *Curves* calculated for a standard set of parameters (below), except for Δg_{iso} (see figure). Experimental values based on $\Phi_T^{av}(0) = 0.22$. (B) Calculated (——) and experimental (*diamonds*) quantum yield anisotropies, $a(H)$, as a function of magnetic field strength. *Curves* calculated for a standard set of parameters (below), except for Δg_{ax} (see figure). The following set of standard parameters were used (see text):

Kinetic: $k_S = 6.5 \times 107\ s^{-1}$, $k_T = 3.5 \times 107\ s^{-1}$;

S-T_0 splitting: $J = 0$, $D/g_e\beta_e = -45$ G, $E/g_e\beta_e = 15$ G,

$$\alpha_D = 0°,\ \beta_D = 90°,\ \gamma_D = 40°;$$

Hyperfine: $A_{iso}/g_e\beta_e = 16$ G, $A_{ax}/g_e\beta_e = 13.1$ G, $\beta_A = 73°$;

Δg: $\Delta g_{iso} = -9 \times 10^{-3}$, $\Delta g_{ax} = 5.7 \times 10^{-4}$, $\Delta g_{rh} = 0$,

$$\alpha_g = 0°,\ \beta_g = 0°.$$

obtained only with very large values of k_T ($\sim 1 \times 10^9$ s^{-1}) (47). As a result, k_S-values of about 2×10^8 s^{-1} are required to fit $\Phi_T(H = 0)$; such values are incompatible with the radical pair decay rate of 9×10^7 s^{-1}. Furthermore, values of k_T greater than 5×10^8 s^{-1} are totally incompatible with the measured high field yield for any value of the g-factor difference (see above). For example, the calculated value of Φ_T increases by 175% on going from 2 to 50 kG when k_T is 5×10^8 in Figure 7, whereas the experimental increase is 136% (Figure 9) (62).

EFFECTS OF ELECTRON-ELECTRON DIPOLAR INTERACTION An anisotropic dipolar interaction has a profound effect on the isotropic quantum yield as a function of field at low field (47). This is easily seen by reference to a radical pair energy level diagram, in which a zero-field splitting of the triplet levels and the orientation dependence of this splitting effectively "spreads out" the energy of the triplet radical pair, in effect placing triplet levels near the singlet level at considerably larger field strengths for particular orientations (this contrasts with the simpler picture in Figure 2). Thus, qualitatively, the rather large $B_{1/2}$ values observed in RCs might be due to this effect. Also, to the extent that $B_{1/2}$ is determined by the dipolar interaction, deuteration may have much less than the expected effect on $B_{1/2}$, though not on the absolute quantum yield. The dependence of the low field quantum yield on various parameters is presented in the following to illustrate their effects. The values of k_S and k_T have each been set at 1×10^8 s^{-1} in the examples that follow. This choice was motivated by the high field data, which are incompatible with much larger values of either parameter. The value of k_T will be discussed further below.

The effect of D for $E = 0$ is shown in Figure 10A. An axial dipolar interaction increases $B_{1/2}$ substantially; however, it also introduces an increase in Φ_T at small fields due to S-T_+ (T_-) level crossing, which is not seen experimentally. The effect of E with $J = 0$ is shown in Figure 10B. Values of $|E|$ close to $(1/3)|D|$ increase the zero-field quantum yield by bringing one of the triplet levels into degeneracy with S at $H = 0$, while not substantially changing the yield at 1000 G. The addition of E also removes an initial rise in the calculated yield with field due to S-T_+(T_-) level crossing by more equally spacing the levels.

EFFECTS OF ELECTRON-ELECTRON EXCHANGE INTERACTIONS The effect of the strength of the exchange interaction varies widely depending upon the particular values of D and E chosen. With $D = E = 0$, increasing $|J|$ decreases the quantum yield and *increases* $B_{1/2}$. With nonzero values of J and D, the field at which the S-T_+(T_-) level crossing occurs depends upon

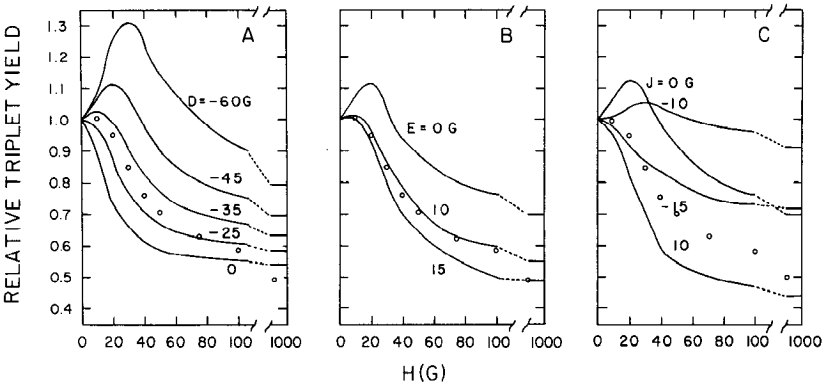

Figure 10 The effect of various parameters on the magnetic field dependence of the triplet quantum yield at low field. *Circles* are experimental values for Q-depleted RCs at 293 K [$\Phi_T(H = 0) = 0.22$]. In each panel, one parameter is varied while the others are kept at the following values:

$$k_T = k_S = 1 \times 10^8\ s^{-1};\quad J = D/g_e\beta_e = -45\ G.$$

$$A_1/g_e\beta_e = -9.5\ G,\ A_2/g_e\beta_e = 13\ G.$$

(A) The effect of the strength of the electron-electron dipolar interaction, D. The calculated zero-field yields are 0.41, 0.29, 0.22, 0.17, and 0.12 for values of $D/g_e\beta_e$ of 0, −25, −35, −45, and −60 G, respectively. (B) The effect of the strength of the nonaxial component of the electron-electron dipolar interaction, E, with $D/g_e\beta_e = -45$ G. The calculated zero-field yields are 0.17, 0.23, and 0.26 for values of $E/g_e\beta_e$ of 0, 10, and 15 G, respectively. (C) The effect of the strength of the isotropic exchange interaction, J. The calculated zero-field yields were 0.13, 0.13, 0.17, 0.31, and 0.34 for values of $J/g_e\beta_e$ of −15, −10, 0, 10, and 20 G, respectively.

orientation, and the effects of these level crossings may not be observable in the average over all orientations. Examples are shown in Figure 10C.

Other Experiments

From the RYDMR linewidth at relatively low power, Norris et al (13f) suggest $k_T = 5.5 \times 10^8\ s^{-1}$. The microwave H_1 field which gives the maximum positive effect gives $J/g_e\beta_e = -16 \pm 4$ G (J defined as in Eq. 1). Consideration of the magnitude of the maximum positive effect and the ratio $\Phi_T(3\ kG)/\Phi_T(H = 0)$ suggests $D/g_e\beta_e = -50 \pm 10$ G. Ogrodnik et al (60) have also obtained a large value for k_T ($7.4 \times 10^8\ s^{-1}$) from an analysis of the time dependent triplet concentration at low field. They find that a dipolar coupling is not required to fit their data.

The discrepancy in k_T is further accentuated by the time-resolved optical data of Parson et al (39), though unfortunately mostly obtained with Q_A^--containing RCs. Even with very large values of k_T, the substantial field dependence of the lifetime could not be modeled with Eq. 13 using the

measured triplet yield. The 6 ns component of delayed fluorescence is a further descrepancy. As measured by optical absorption, the radical pair is formed in approximately 100% yield in less than 4 ps (31) and decays in 11 ns. This fluorescence lifetime data led Parson and co-workers to suggest that the radical pair relaxes in some way in 6 ns and is nonfluorescent for the remainder of its 11 ns lifetime.

To help resolve these discrepancies we have recently measured the radical pair decay kinetics at 0, 1 and 50 kG (62a). We find the decay to be exponential within experimental error, with lifetimes of 13 ± 1 ns at $H = 0$, 17 ± 2 ns at $H = 1$ kG, and 9 ± 2 ns at $H = 50$ kG. This result suggests a large value of k_T and is inconsistent with the measured absolute triplet quantum yield.

DISCUSSION

The analysis of magnetic field effects in RCs touches on nearly all aspects of the effects that spin dynamics can exert on a chemical reaction. CIDNP and CIDEP share much of the theoretical background with the RC problem, but diffusion eliminates the need to consider dipolar and other anisotropic magnetic interactions. The quantum yield anisotropy effects, discovered in RCs, are a dramatic example of the consequences of preserving the spatial relationship between the radicals in the pair during their lifetime. The anisotropy and its field dependence can be exquisitely sensitive to the radical pair structure. There are many interesting physical situations intermediate between the solid state situation in RCs and radical pair reactions in fluid solution. Reactions in highly viscous solution or contained within or on the surface of micelles or vesicles are two examples.

Magnetic field effects have most often been studied at low field; unfortunately, low field is also the most difficult to treat without making approximations that may mask key interactions. The high field limit is much more amenable to rigorous calculation. Also, the S-T mixing rate, ω, can be changed without limit by going to higher and higher field (if $\Delta g \neq 0$), providing a useful experimental variable. The plots in Figures 7–10 illustrate the diversity of effects the various kinetic and magnetic parameters manifest in the field dependence of the triplet yield.

The intense level of interest in the primary photochemistry of photosynthesis is, of course, driven by the singular importance of this reaction. Photosynthesis offers chemically interesting and sometimes unique phenomena, including the magnetic field effects. The analysis of these effects offers mechanistic insight, as well as specific data on the electronic coupling and three-dimensional relationship of the reactive components.

In the following two implications of the magnetic field effects are discussed.

First, the value of $\Delta g_{iso} = -10 \times 10^{-4}$ obtained by modeling the high field effects agrees very well with the value $\Delta g_{iso} = 2.0026 - 2.0035 = -9 \times 10^{-4}$ obtained from EPR studies of P^{+} and I^{-} (54, 55). This supports the claim (55) that the species trapped at low temperature in RCs and observed by EPR on a slow time scale is the same as that which exists in the radical pair $(P^{+}I^{-})$ on the ns time scale. The theory used for Q-depleted RCs assumes the hyperfine mechanism to be the only source of S-T mixing at low fields. As the values of k_S, k_T, J, $\mathscr{D}$, Δg, and the hyperfine interactions can all be simultaneously scaled with no effect on the predicted triplet yield or its magnetic field dependence in the high field limit, these results can alternatively be taken as support for the hyperfine mechanism of S-T mixing. That is the magnetic field dependence of the triplet yield is compatible with the relative values of Δg_{iso} and the hyperfine interactions measured by EPR. We have demonstrated that the change of $B_{1/2}$ on deuteration is an unreliable probe of the hyperfine mechanism in RCs, in sharp contrast to the Py-Dma case. Furthermore, even the dependence of the absolute yield on deuteration may not be a reliable probe of mechanism, as deuteration is known to affect kinetic characteristics greatly; e.g. the radical pair lifetime changes significantly on deuteration for unknown reasons (39).

The second issue involves the values of the rate constant k_T obtained by different methods: the RYDMR experiments of Norris and co-workers (13f), the time-resolved low field dependence measurements of Ogrodnik et al (60), and our observation that the radical pair lifetime decreases on going from 1 to 50 kG (62a) require large values of k_T on the order of $5 \times 10^8\ s^{-1}$; however, the high field triplet quantum yield data require $k_T < 1 \times 10^8\ s^{-1}$. This conflict in values for k_T is especially interesting because the theories used to analyze the results of all four types of experiments are essentially the same. Thus, we are forced to consider the possibility that the scheme in Figure 3B is not complete. A possible resolution of the conflict is the following: If there were another decay channel, the limiting quantum yield could be less than $k_T/(k_S + k_T)$, and the estimate for k_T from the high field dependence would be too low. The notion that other decay pathways should be included in Figure 3B has been stressed by Parson and co-workers (39) in their attempt to rationalize the triplet yield and radical pair decay and fluorescence data. The nature of this pathway and the mechanism that determines the branching ratio remain obscure. The magnetic field effect and RYDMR data do demonstrate that all elements in the present scheme are required as part of any complete analysis of the primary photochemistry of photosynthesis.

ACKNOWLEDGMENTS

The authors wish to thank Professors Closs, Haberkorn, Michel-Beyerle, Parson, and Schulten, and Doctors Norris and Tang for helpful discussions. The work in the authors' laboratory was supported by NSF and USDA/CRGO/SEA Grants PCM7926677 and 78-59-2066-0-1, respectively. C.E.D.C. is an NSF and John and Fannie Hertz Fellow. S.G.B. is an A. P. Sloan and Camille and Henry Dreyfus Teacher-Scholar Fellow.

Literature Cited

1. Molin, Yu. N., Sagdeev, R. Z., Salikhov, K. M. 1979. *Sov. Sci. Rev. Sect. B Chem. Rev.* 1:1–67
2. Sagdeev, R. Z., Salikhov, K. M., Molin, Yu. M. 1977. *Russ. Chem. Rev.* 46:297–315
3. Atkins, P. W., Lambert, T. P. 1975. *Ann. Rep. Prog. Chem. Sect. A Phys. Inorg. Chem.* 72:67–88
4. Lepley, A. R., Closs, G. L., eds. 1973. *Chemically Induced Magnetic Polarization.* New York: Wiley
5. Muus, L. T., Atkins, P. W., McLauchlan, K. A., Pedersen, J. B., eds. 1977. *Chemically Induced Magnetic Polarization.* Boston: Reidel
6. Avakian, P. 1974. *Pure Appl. Chem.* 37:1–19
7. Faulkner, L. R., Tachikawa, H., Bard, A. J. 1972. *J. Am. Chem. Soc.* 94:691–99
8. Schulten, K., Staerk, H., Weller, A., Werner, H.-J., Nickel, B. 1976. *Z. Phys. Chem. NF* 101:371–90
9. Michel-Beyerle, M. E., Haberkorn, R., Bube, W., Steffens, E., Schroder, H., Neusser, H. J., Schlag, E. W., Seidlitz, H. 1976. *Chem. Phys.* 17:139–45
10. Werner, H.-J., Schulten, Z., Schulten, K. 1977. *J. Chem. Phys.* 67:646–63
11. Werner, H.-J., Staerk, H., Weller, A. 1978. *J. Chem. Phys.* 68:2419–26
12. Schulten, K., Wolynes, P. G. 1978. *J. Chem. Phys.* 68:3292–97
13. Michel-Beyerle, M. E., Kruger, H. W., Haberkorn, R., Seidlitz, H. 1979. *Chem. Phys.* 42:441–47

13a. Thurnauer, M. C., Katz, J. J., Norris, J. R. 1975. *Proc. Natl. Acad. Sci. USA* 72:3270–74

13b. Gast, P., Hoff, A. J. 1979. *Biochim. Biophys. Acta* 548:520–35

13c. Frankevich, E. L., Pristupa, A. I. 1976. *Pis'ma Zh. Eksp. Teor. Fiz.* 24:397–400

13d. Frankevich, E. L. 1980. *High Energy Chem.* 14:143–56

13e. Bowman, M. K., Budil, D. E., Closs, G. L., Kostka, A. G., Wraight, C. A., Norris, J. R. 1981. *Proc. Natl. Acad. Sci. USA* 78:3305–7

13f. Norris, J. R., Bowman, M. K., Budil, D. E., Tang, J., Wraight, C. A., Closs, G. L. 1982. *Proc. Natl. Acad. Sci. USA* 79:5532–36

14. Buchachenko, A. L. 1977. *Russ. J. Phys. Chem.* 52:1445–51
15. Turro, N., Kraeutler, B. 1980. *Acct. Chem. Res.* 13:369–77
16. Sterna, L., Ronis, D., Wolfe, S., Pines, A. 1980. *J. Chem. Phys.* 73:5493–99
17. Biegelsen, D. K., Knights, J. C., Street, R. A., Tsang, C., White, R. M. 1978. *Philos. Mag. B* 37:477–88
18. Deleted in proof
19. Street, R. A. 1982. *Phys. Rev. B* 26:3588–3604
20. Haberkorn, R., Dietz, W. 1980. *Solid State Commun.* 35:505–8
21. Bube, W., Michel-Beyerle, M. E., Haberkorn, R. A., Steffens, E. 1977. *Chem. Phys. Lett.* 50:389–93
22. Remsen, C. C. 1978. In *The Photosynthetic Bacteria*, ed. R. K. Clayton, W. R. Sistrom, pp. 31–60. New York: Plenum
23. Clayton, R. K. 1980. *Photosynthesis: Physical Mechanisms and Chemical Patterns.* New York: Cambridge Univ. Press
24. Feher, G., Okamura, M. Y. 1978. See Ref. 22, pp. 349–86
25. Hoff, A. J. 1979. *Phys. Rep.* 54:77–200
26. Rockley, M. G., Windsor, M. W., Cogdell, R. J., Parson, W. W. 1975. *Proc. Natl. Acad. Sci. USA* 72:2251–55
27. Kaufmann, K. J., Dutton, P..L., Netzel, T. L., Leigh, J. S., Rentzepis, P. M. 1975. *Science* 188:1301–4
28. Dutton, P. L., Kaufmann, K. J., Chance, B., Rentzepis, P. M. 1975. *FEBS Lett.* 60:275–80
29. Peters, K., Avouris, Ph., Rentzepis, P. M. 1978. *Biophys. J.* 23:207–17
30. Moskowitz, E., Malley, M. M. 1978. *Photochem. Photobiol.* 27:55–59
31. Holten, D., Hoganson, C., Windsor, M. W., Schenck, C. C., Parson, W. W., et al.

1980. *Biochim. Biophys. Acta* 592:461–77
32. Wraight, C. A., Clayton, R. K. 1973. *Biochim. Biophys. Acta* 333:246–60
33. Schenck, C. C., Parson, W. W., Holten, D., Windsor, M. W., Sarai, A. 1981. *Biophys. J.* 36:479–89
34. Vermeglio, A., Clayton, R. K. 1977. *Biochim. Biophys. Acta* 461:159–65
35. Arata, H., Parson, W. W. 1981. *Biochim. Biophys. Acta* 636:70–81
36. Parson, W. W. 1978. See Ref. 22, pp. 455–69
37. Dutton, P. L., Leigh, J. S., Reed, D. W. 1973. *Biochim. Biophys. Acta* 292:654–64
38. Levanon, H., Norris, J. R. 1978. *Chem. Rev.* 78:185–98
39. Schenck, C. C., Blankenship, R. E., Parson, W. W. 1982. *Biochim. Biophys. Acta* 680:44–59
40. Blankenship, R. E., Schaafsma, T. J., Parson, W. W. 1977. *Biochim. Biophys. Acta* 461:297–305
41. Hoff, A. J., Rademaker, H., van Grondelle, R., Duysens, L. N. M. 1977. *Biochim. Biophys. Acta* 460:547–54
42. Werner, H.-J., Schulten, K., Weller, A. 1978. *Biochim. Biophys. Acta* 502:255–68
43. Haberkorn, R., Michel-Beyerle, M. E. 1979. *Biophys. J.* 26:489–98
43a. Hoff, A. J. 1981. *Q. Rev. Biophys.* 14:599–665
44. Blankenship, R. E., Parson, W. W. 1979. *Biophys. J.* 25:205a
45. Chidsey, C. E. D., Roelofs, M. G., Boxer, S. G. 1980. *Chem. Phys. Lett.* 74:113–18
46. Boxer, S. G., Chidsey, C. E. D., Roelofs, M. G. 1982. *J. Am. Chem. Soc.* 104:1452–54
47. Roelofs, M. G., Chidsey, C. E. D., Boxer, S. G. 1982. *Chem. Phys. Lett.* 87:582–88
48. Boxer, S. G., Chidsey, C. E. D., Roelofs, M. G. 1982. *J. Am. Chem. Soc.* 104:2674–75
49. Boxer, S. G., Chidsey, C. E. D., Roelofs, M. G. 1982. *Proc. Natl. Acad. Sci. USA* 79:4632–36
50. Gordy, W. 1980. *Theory and Applications of Electron Spin Resonance.* New York: Wiley
51. Redfield, A. G. 1965. *Adv. Magn. Reson.* 1:1–32
52. Freed, J. H., Pedersen, J. B. 1976. *Adv. Magn. Reson.* 8:1–84
53. Edmonds, A. R. 1974. *Angular Momentum in Quantum Mechanics*, p. 6. Princeton: Princeton Univ. Press
54. McElroy, J. D., Feher, G., Mauzerall, D. C. 1972. *Biochim. Biophys. Acta* 267:363–74
55. Okamura, M. Y., Isaacson, R. A., Feher, G. 1979. *Biochim. Biophys. Acta* 546:394–417
56. Tang, J., Norris, J. R. 1982. *Chem. Phys. Lett.* 92:136–40
57. Haberkorn, R., Michel-Beyerle, M. E., Marcus, R. A. 1979. *Proc. Natl. Acad. Sci. USA* 76:4185–88
58. Butler, W. F., Johnston, D. C., Shore, H. B., Fredkin, D. R., Okamura, M., Feher, G. 1980. *Biophys. J.* 32:967–92
58a. Tang, J., Norris, J. R. 1983. *Chem. Phys. Lett.* 84:77–80
58b. Lersch, W., Ogrodnik, A., Michel-Beyerle, M. E. 1982. *Z. Naturforsch. A* 37:1454–56
59. Roelofs, M. G. 1982. PhD thesis. Stanford Univ., Stanford, Calif.
60. Ogrodnik, A., Kruger, H. W., Orthuber, H., Haberkorn, R., Michel-Beyerle, M. E., Scheer, H. 1982. *Biophys. J.* 39:91–99
61. Cantor, C. R., Schimmel, P. R. 1980. *Biophysical Chemistry*, Pt. 2, Ch. 8, pp. 457–59. San Francisco: Freeman
62. Michel-Beyerle, M. E., Scheer, H., Seidlitz, H., Tempus, D., Haberkorn, R. 1979. *FEBS Lett.* 100:9–12
62a. Chidsey, C. E. D., Kirmaier, C., Holten, D., Boxer, S. G. 1983. *Biochim. Biophys. Acta.* In press